Including Radiative Heating for the Design of the Orion Backshell for Artemis-1: A Narrative

Christopher O. Johnston
NASA Langley Research Center, Hampton, VA 23681

I. Introduction

The shock-layer radiative heating to the backshell of Earth entry vehicles at velocities greater than 10 km/s was ignored during all NASA thermal protection system (TPS) designs prior to 2015, even for conditions where radiative heating to the forebody was considered (see Fig. 1 for a definition of the forebody and backshell regions of the Orion geometry). In the 2014-2015 timeframe, a study by Johnston and Brandis [1] identified the potential for backshell radiative heating being significant, relative to convective heating, for Earth entry vehicles at velocities greater than 10 km/s. The significance of this discovery to the backshell heating for the Orion capsule during the Artemis-1 mission was quickly recognized (Note that the previous Orion EFT-1 mission had an entry velocity below 9 km/s, so this backshell radiation component was not important). This late identification, in 2014, of the backshell radiative heating left only a few months for its inclusion during the final TPS design for the Artemis-1 backshell, which was then considering only convective heating.

In response, a database of backshell radiative heating values was rapidly compiled using the LAURA flowfield and HARA radiation codes. These backshell radiative heating values were then added to the existing convective heating database, with the combined convective and radiative heating used for the Orion backshell TPS sizing for the Artemis-1 mission. Note that this design for the un-crewed Artemis-1 mission was also used for the subsequent crewed Artemis-2 and later missions, which emphasizes the importance of this design. Between the backshell TPS sizing in 2015 and the flight of Artemis-1 in 2022, the legitimacy of this radiative heating component remained questionable, due to the complexity of the backshell radiation modeling and lack of relevant measurements. The Artemis-1 flight in late 2022 provided measurements inferring that radiative heating was the dominant heating mechanism on regions of the lee-side backshell, therefore confirming the importance of its inclusion in the design process.

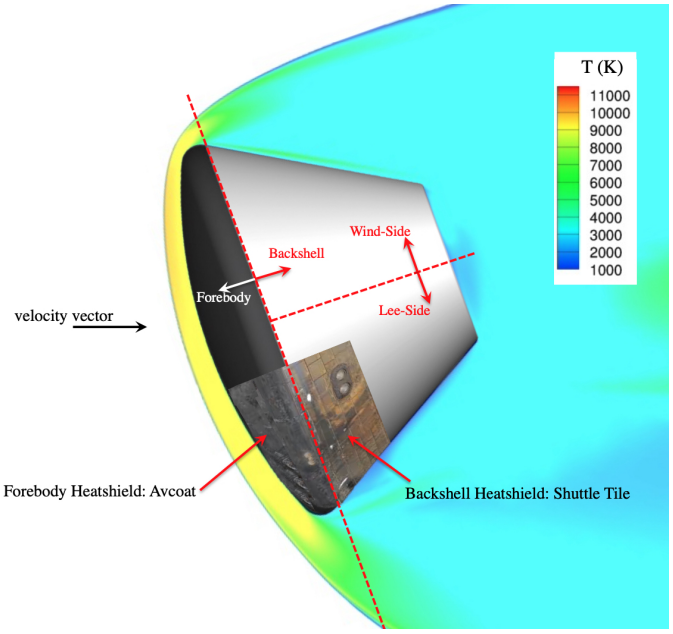

Fig. 1 Definition of forebody and backshell regions for a simplified Orion capsule.

Further details of this story are presented in this paper, which provides a narrative history of backshell radiative heating for Earth entry. This begins in Section II with a discussion of how the erroneous assumption of negligible radiative heating originated. The identification of backshell radiation being an important component is presented in Section III. Section IV discusses the process of relatively quickly developing a state-of-the-art radiative heating database for the design of the Orion backshell for Artemis-1. Between the completion of the radiation database in 2015 and the Artemis-1 flight in 2022, a number of relevant studies were performed to better understand this backshell radiation component, which are discussed in Section V. Finally, Section VI compares the radiative and convective heating used for design with the total heating inferred from the Artemis-1 thermocouple measurements. This comparison will highlight the importance of the nearly-missed radiative heating component to the design of the Orion backshell TPS.

II. Origins of the Negligible Backshell Radiative Heating Assumption

Radiative heating has long been considered a contributor to the stagnation region heating of Earth entry vehicles at velocities greater than 10 km/s [2]. However, for all NASA missions prior to 2014 the backshell radiative heating was assumed negligible. For example, the radiative heating for Apollo was computed at the stagnation region and assumed to decrease away from this point to a value of zero at the shoulder [3]. The assumption of negligible backshell radiative heating for Earth entry at velocities greater than 10 km/s is a consequence of three Apollo-era legacies. These three legacies are presented in the following subsections, where the first two provide the justification for the negligible backshell radiative heating assumption, while the third indicates why assumption was adequate for Apollo (and Stardust). As presented in these subsections, the assumption of negligible backshell radiation appears justified. The erroneous aspects of each of these legacies will be identified in Section III, which lead to the discovery of the backshell radiation component.

A. Negligible Apollo 4 and Fire II Backshell Radiometer Values

The Fire II and Apollo 4 tests represent two successful measurements of the radiative heating to Earth entry vehicles at velocities greater than 10 km/s [3, 4]. Fire II was performed early enough to inform the late stage of the Apollo design, while Apollo 4 was used for certification prior to crewed flights. The backshell radiometers for both Apollo 4 and Fire II were placed behind quartz windows. These windows were known to absorb radiation below 200 nm, which is the vacuum ultraviolet (VUV) region of the spectrum. While this absorption is not ideal, it was deemed acceptable because experience with radiation on the forebody indicated that there are roughly equal contributions from wavelengths above and below 200 nm. An example of this is shown in Fig. 2, which presents a representative stagnation region spectrum near peak heating. The cumulative curve shows that the wavelength-integrated contribution above and below 200 nm have similar magnitudes. Assuming this trend held for backshell radiation, the Fire II and Apollo 4 measurements of only the component above 200 nm would provide a useful metric for assessing the magnitude of backshell radiative heating.

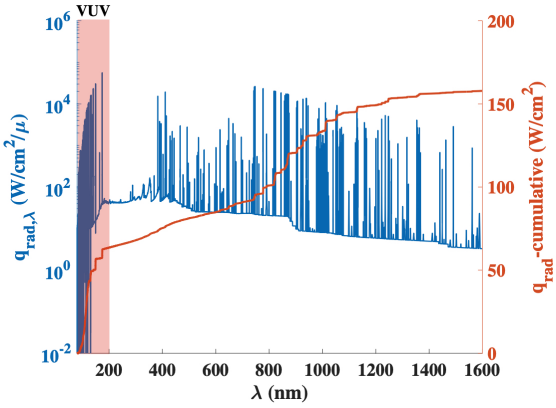

Fig. 2 Stagnation region spectrum showing the similar contributions above and below 200 nm.

The result of these flight tests were radiometer measurements of essentially zero. Assuming the VUV and non-VUV components were nearly equal, these measurements suggested the backshell radiative heating was negligible. This

result agreed with the simulations at the time [5], which applied the Boltzmann assumption, as discussed in the next subsection. This agreement provided the rationale needed for ignoring backshell radiative heating for Apollo.

B. Boltzmann Radiation Limit

The nonequilibrium radiation component to a vehicle forebody is a result of the compressing nonequilibrium post-shock flow. Because, unlike backshell radiation, forebody radiation has always been considered for Earth entry above 10 km/s, the radiation from a compressing nonequilibrium post-shock flow has been studied considerably, as summarized by Park [6]. For Apollo, post-shock emission measurements from shock tubes were scaled and added to the equilibrium contribution to provide the design heating for the forebody [3]. This equilibrium radiation assumes that the species composition are equal to the chemical equilibrium values at the local pressure and temperature, while the electronic levels (which most strongly impact the radiation) are equal to their Boltzmann values. The Boltzmann values are only dependent on the number density of the radiating species and the electronic temperature (which is typically grouped with the vibrational and free-electron temperature).

As thermochemical nonequilibrium flowfield simulations were developed in the 1980s and 1990s [7–10], the chemical equilibrium assumption was removed. To remove the Boltzmann assumption when computing radiation from these flowfields, Chul Park pioneered non-Boltzmann radiation models [11, 12], which solved for the electronic state populations of radiating atoms and molecules. While the development of the nonequilibrium radiation modeling by Park was a significant advancement in the state-of-the-art for radiation modeling, it was known that the radiation predictions resulting from these models contained significant uncertainty. This significant uncertainty is primarily a result of the model requiring the estimation of numerous rates (on the order of hundreds for atoms). Park estimated these rates with various approaches and tuned them to match the limited available experimental data [13, 14]. Another challenge and source of uncertainty with non-Boltzmann models is capturing the impact of non-local absorption on the level populations, which is approximated with the so-called escape factor approach [15].

Developed in the late 1990s, Stardust was NASA's first post-Apollo Earth entry at a velocity greater than 10 km/s. By this time, thermochemical nonequilibrium flowfields were available for the radiative heating simulations. Because of the large non-Boltzmann modeling uncertainty, the assumed conservatism of the Boltzmann assumption, and the added computational expense of non-Boltzmann models, the Boltzmann assumption was applied for Stardust's design radiative heating values [16]. These Boltzmann radiative heating values were negligible relative to convective heating on the backshell. Therefore, this Stardust design reinforced the negligible backshell radiation assumption that started with Apollo. Fortunately for the success of Stardust, the backshell convective heating values were multiplied by a factor of 3.5x to account for turbulence and angle of attack effects. In retrospect, this multiplication factor on the convective heating bounded the unknown radiative heating contribution to avoid an under-designed backshell TPS for Stardust.

Although the present narrative focuses on NASA applications, JAXA's Hayabusa capsule, which had an entry velocity greater than 10 km/s, was developed in the late 1990s and early 2000s. The radiation code developed by Fujita et al. [17] was used for Hayabusa design, which cites the use of a Boltzmann distribution. The resulting backshell radiation presented by Otsu [18] shows small backshell radiation values for air species, but shows a large backshell radiation component when ablation products are accounted for. Ironically, the Boltzmann assumption for the ablation product emission results in the upper limit of the ablation product emission, even in the backshell, similar to forebody atomic emission. Based on current non-Boltzmann modeling of ablation products, their contribution to backshell radiation is small. This large impact of ablation product emission to backshell radiation was not adopted by future NASA studies, although perhaps this result should have motivated a closer analysis of backshell radiation.

The original best practices for the radiative heating simulations for Orion were developed in the late 2000s [19] and followed the lessons learned from Apollo and Stardust, where Stardust had a successful entry in 2006. Applying the Park non-Boltzmann model [11] resulted in radiative heating values that were consistently negligible relative to convective heating. Furthermore, when the Boltzmann option was engaged, the resulting values remained negligible relative to convective heating. This negligible radiation from the Boltzmann assumption, which avoided the uncertainty of the nonequilibrium model and was assumed to represent the upper limit, provided an apparently conclusive indication that backshell radiation was negligible.

C. Avcoat used for Apollo Backshell TPS

The backshell TPS for Apollo was composed of Avcoat [20], with thicknesses varying from 0.7 to 1.5 inches [21]. This is the same charring ablator material used for Apollo's forebody heatshield, which had thicknesses varying from 2.0 to 2.7 inches [21]. As discussed by Pavlosky and Leger [21], this conservative design of the backshell TPS was a

result of uncertainties in flowfield modeling at the time. The uncertainties in the flowfield modeling were due to the lack of CFD capable of simulating the separated flow environments characteristic of much of the backshell flowfield, which prevented the convective or radiative heating from being simulated. Instead of relying on simulations, the backshell convective heating was estimated based on correlations of wind tunnel measurements [22]. The backshell radiative heating, however, was assumed equal to zero. Nevertheless, Pavlosky and Leger note that the possibility of non-negligible radiative heating was another reason, in addition to uncertainties in flowfield modeling, for the conservative design of the backshell TPS. Based on their nominal heating values, which treat convective heating only, Pavlosky and Leger mention that metal shingles were a feasible backshell TPS. However, note that the metal shingles on the backshell of Gemini 2 experienced burn-through [23, 24] due to higher than expected convective heating levels, which perhaps encouraged the conservative design for Apollo.

By design, Apollo's conservative Avcoat TPS was more than capable of handling the potentially unknown radiative heating component. In fact, in the TPS certification for the first crewed lunar return mission (Apollo 8) [25], the Apollo un-crewed flight measurements of the backshell heating were noted to be under-predicted on the lee-side backshell by the convective heating model used for design. This was addressed by ensuring that the as-built backshell TPS could withstand lee-side backshell heating that was 6% of the stagnation point convective heating. This conservative approach for resolving the discrepancy with measurements was possible because of the presence of Avcoat on the backshell, which was capable of handling the resulting higher heating values.

The higher heating capability of Avcoat (above 100 W/cm^2) also influenced the magnitude of what was considered a negligible radiative heating value. The 6% of the stagnation point convective heating noted above for the lee-side backshell results in heating values above 20 W/cm^2, which remains a low value for Avcoat. This influenced setting the noise floor of roughly 2 W/cm^2 for the Fire II backshell radiometer [4], where a heating value of 2 W/cm^2 was considered negligible. For a less capable TPS, such as the Shuttle tile used for the Orion backshell for Artemis-1 [26], heating values down to 1 W/cm^2 are meaningful.

In summary, the use of Avcoat as the backshell TPS for the successful Apollo program obfuscated inadequacies in the expected heating environments, and therefore ignoring the backshell radiation component (based on the justifications provided in subsections II.A and II.B) was inconsequential (note that, as discussed in subsection II.B, Stardust avoided the same issue with a 3.5x multiplier on the backshell convective). However, for Orion the weight penalty associated with an Avcoat backshell (or a similarly robust TPS) is not acceptable (note that the surface area of the backshell is significantly larger than the forebody), so Shuttle tile was chosen [26], which is lighter but less capable of handling high heating. Therefore, the Apollo (or Stardust) approach that avoided quantifying the backshell heating levels could not be taken for Orion.

III. Identifying the Importance of Backshell Radiative Heating

The development that ultimately led to the identification of the backshell radiative heating component was the reassessment of the non-Boltzmann models for electronic levels for atomic nitrogen performed by Johnston et al. [27]. The updated non-Boltzmann rates were implemented in the HARA radiation code, which was developed in the late 2000s. This study represented the first reassessment of these rates since the original developments by Park [11], and since then, advancements in computational chemistry provided improved estimation of many of the rates [28, 29]. Figure 3 compares the heritage rate from Park with the values computed from computational chemistry, where HARA applies the values from Frost [28]. Although it was not recognized at the time of its development, this reassessed rate model produces higher backshell radiative heating than previous models, which will be discussed further at the end of this section.

The Osiris-Rex capsule was designed to have the same geometry and TPS as Stardust, as well as to experience similar entry conditions [30]. Therefore, following the Stardust experience cited in Section II.B, the backshell radiative heating was expected to be negligible. In late 2013 and early 2014 Jarvis Songer of Lockheed Martin used the LAURA flowfield and HARA radiation codes to assess the Osiris-Rex heating. From these simulations he noticed radiative heating values at a backshell seal location that were larger than the convective heating. This surprising result was assumed erroneous at first based on the reasons discussed in the previous section. However, this result motivated the detailed study presented by Johnston and Brandis [1], which provided evidence that this radiative heating was legitimate.

The primary questions addressed by Johnston and Brandis [1] relate to the two assumptions that led to the backshell radiation being ignored: the negligible Fire II and Apollo 4 backshell radiometer measurements and the negligible Boltzmann predictions. These two issues may both be explained by considering the nonequilibrium electronic state population for atomic nitrogen at a point in the backshell flowfield, and contrast this distribution with one in the forebody

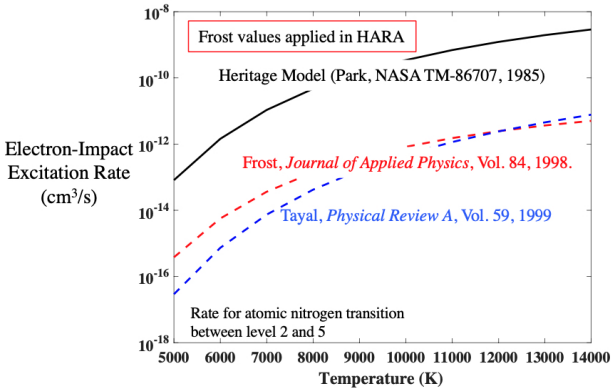

Fig. 3 Example comparison of non-Boltzmann rate differences used in the development of HARA.

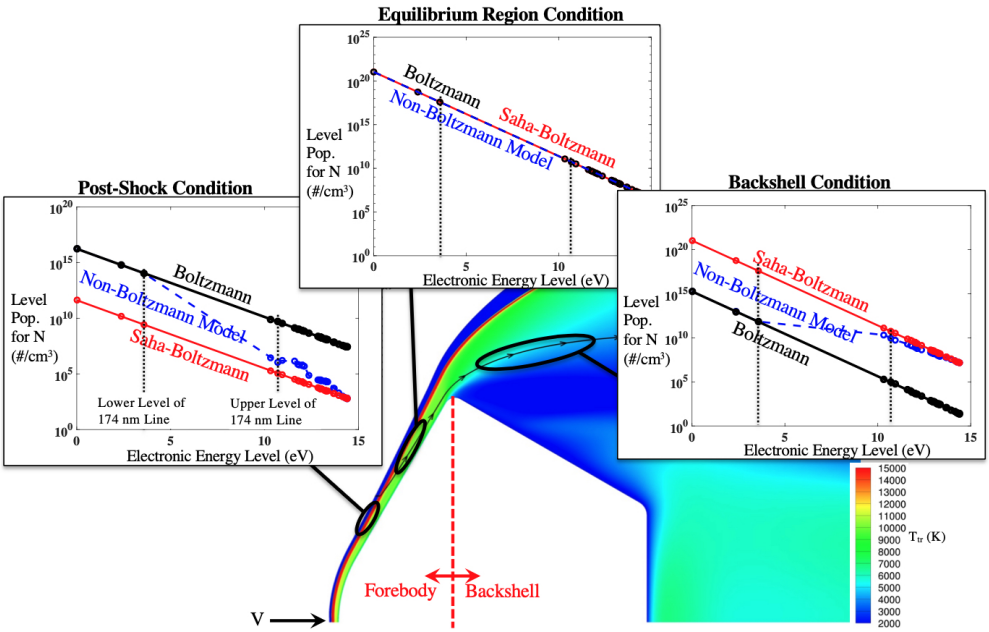

Fig. 4 Overview of differences in electronic level population of atomic species between the forebody and backshell.

flowfield. To pursue this, Fig. 4 presents a streamline passing through the bow shock of a Stardust capsule and flowing into the backshell flowfield (the Stardust capsule is shown for simplicity, although the same figure can be made for Orion). In the immediate post-shock region, the compressing flow is ionizing while also exciting the electronic states of newly-formed N to higher energy levels. The finite rate ionization and excitation processes prevent the populations of higher energy levels from reaching their local equilibrium values represented by the local electronic temperature (T_{ve}) and total number density of N (N_a), which is the Boltzmann distribution. Figure 4 shows that in the post-shock non-Boltzmann population distribution, the higher energy level populations (at energy levels above 10 eV) are below the Boltzmann limit. At the highest energy levels, these populations converge to the Saha-Boltzmann distribution. Because the radiative emission is proportional to the population of higher levels, this post-shock distribution confirms the previously stated assumption that treating the higher level populations using the Boltzmann distribution results in an upper limit on the radiation.

This assumption remains valid when moving into the equilibrium region of the shock layer, where the Boltzmann, Saha-Boltzmann, and Non-Boltzmann model all converge to the same distribution (by definition, the Boltzmann and Saha-Boltzmann become identical at chemical equilibrium). This equilibrated flow becomes unequilibrated,

however, when the streamline reaches the quickly decreasing pressure of the shoulder expansion. The translational and free-electron temperatures are able to equilibrate to these lower pressures quickly; however, the recombination process (reverse of the ionization process) between electrons, ions, and neutral species is not able to equilibrate. This means that the number densities of electrons and ions will be larger than the value suggested by chemical equilibrium at the local pressure and temperature. As shown in the population distribution for the backshell condition in Fig. 4, this results in the Saha-Boltzmann distribution being larger than the Boltzmann distribution. Similarly to the post-shock condition, the higher level populations predicted by the non-Boltzmann model converge to the Saha-Boltzmann distribution, while the lower three levels remain close to the Boltzmann distribution. This means that the only difference between the backshell and post-shock conditions is that, for the backshell condition, the Saha-Boltzmann distribution is larger than the Boltzmann distribution, rather than smaller. The consequence of this observation is that the Boltzmann distribution now represents the lower population limit of the emitting higher levels, which is opposite of the assumed Boltzmann upper-limit discussed in Section II.B. This provides the reason that the simulations performed in the past for backshell radiation, which assumed a Boltzmann distribution for conservatism (and to avoid perceived inadequacies in earlier non-Boltzmann models) were predicting negligible backshell radiation.

The next question to address is why the Apollo 4 and Fire II backshell radiometers measured negligible radiation. Because the quartz window in front of these radiometers absorbed out the vacuum ultraviolet (VUV) component of the spectrum, the answer to this question requires showing that this VUV component that was not captured in the measurement provides the dominant radiative heating contribution. This behavior would be in contrast to that observed in the forebody region, where the VUV and non-VUV contributions are of similar magnitude. To investigate the VUV radiation, consider the radiative intensity at the center of an optically-thick atomic line, which is written (ignoring induced emission, which is negligible for VUV lines) as

$$I_{\lambda,Limit} = \frac{2hc^2}{\lambda^5}\frac{N_u N_L^B}{N_L N_u^B} exp\left(-\frac{hc}{kT_{ve}}\frac{1}{\lambda}\right) \tag{1}$$

where the superscript B indicates a Boltzmann distribution and N_u and N_L are the number densities of the upper and lower levels for the atomic line, respectively.

The defining characteristic of VUV lines is that they are located below 200 nm. Recall that the centerline wavelength of an atomic line is defined by the inverse of the energy difference between its upper and lower levels ($\lambda_{CL} = 1/(E_u - E_L)$). In N and O, the only energy level difference between an upper and lower level that is large enough to drive the wavelength below 200 nm is between an upper level above 10 eV and a lower level below 5 eV. For example, the levels corresponding to the 174 nm N line are identified in Fig. 4 by dotted lines. This figure shows that for a backshell condition, the upper level may be approximated by the Saha-Boltzmann distribution while the lower level is approximated by the Boltzmann distribution. This allows Eq. (1) to be approximated as follows for a VUV line:

$$I_{\lambda,Limit,VUV} = \frac{2hc^2}{\lambda^5}\frac{N_u^{SB}}{N_L^B} exp\left(-\frac{hc}{kT_{ve}}\frac{1}{\lambda}\right) \tag{2}$$

where the ratio N_u^{SB}/N_u^B represents the separation between the Boltzmann and Saha-Boltzmann distributions seen in Fig. 4. This VUV atomic line component therefore increases as the Saha-Boltzmann values become larger than the Boltzmann values.

In contrast to VUV lines, the non-VUV lines must have upper and lower levels that are both located above 10 eV. This is required for the inverse of the energy level difference to result in wavelengths greater than 200 nm (there are no emitting transitions between the three levels below 5 eV for either N or O). Figure 4 shows that for the backshell condition, the Saha-Boltzmann distribution would therefore be applied to approximate both the upper and lower levels for non-VUV lines. Applying this to Eq. (1) results in the following:

$$I_{\lambda,Limit,non-VUV} = \frac{2hc^2}{\lambda^5} exp\left(-\frac{hc}{kT_{ve}}\frac{1}{\lambda}\right) \tag{3}$$

which is the Planck function ignoring induced emission. Comparing Eqs. (2) and (3) shows that the VUV and non-VUV limits differ by the factor N_u^{SB}/N_u^B. This factor is orders-of-magnitude larger than 1.0 in the backshell, as shown in Fig. 4, which means the VUV radiation component will be significantly larger than the non-VUV component. This explains why the VUV component is dominant for backshell radiation, and implies that this component was present for Apollo 4 and Fire II, but was simply absorbed by the quartz window, which was known to absorb the VUV component.

Figure 5 confirms this with the simulated backshell spectrum for the Fire II peak heating case, which shows that only 1.4 W/cm^2 of the total 6.5 W/cm^2 was present above 200 nm. This 1.4 W/cm^2 is below the noise floor cited for the measurement [4]. For the forebody, which is mostly equilibrium dominated, the N_u^{SB}/N_u^B ratio is near 1.0, which explains the nearly equal VUV and non-VUV components typically assumed and shown in Fig. 2.

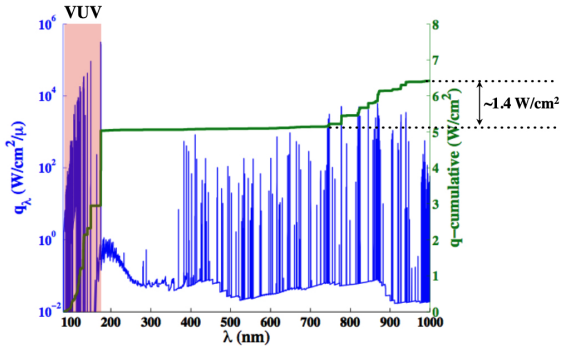

Fig. 5 Backshell spectrum for Fire II showing the dominance of the region below 200 nm.

The conclusions reached in the above discussion apply the Saha-Boltzmann as a surrogate for the non-Boltzmann model for energy levels above 5 eV. This assumption was appropriate for deriving Eqs. (2) and (3) to show the dominance of VUV lines and that the Boltzmann assumption represented the lower radiation limit at backshell conditions. However, note that this assumption is not adequate for accurate radiation simulations, which require the non-Boltzmann modeling results. For example, the populations in Fig. 4 are plotted on logarithmic scale, so the exact values of the non-Boltzmann model may differ from the Saha-Boltzmann distribution by over an order-of-magnitude. As discussed, significant uncertainty remains in the non-Boltzmann model. The updated non-Boltzmann rates discussed with Fig. 3 resulted in upper level populations significantly larger than the previous Park model, which caused the resulting radiative heating to rise from negligible to meaningful levels. This is shown in Fig. 6, which compares the electronic state populations for N resulting from the updated HARA non-Boltzmann model and the original Park model. A backshell relevant condition is considered: T_{ve}=5000 K, N_a=8×10^{15} #/cm^3, N_e=5×10^{14} #/cm^3, N_+=4×10^{14} #/cm^3. Although on the logarithmic scale, the two non-Boltzmann distributions appear relatively close, the population of the 5th level (which is defined slightly differently between the two models), which controls the emission from the 174 nm line, is a factor of 5 larger for the HARA model than the Park model. This difference is enough to increase the backshell radiation from a negligible to a significant value. The differences become even larger when differences in the non-local absorption (escape factor) modeling are accounted for, where Fig. 6 assumes escape factors of zero for simplicity.

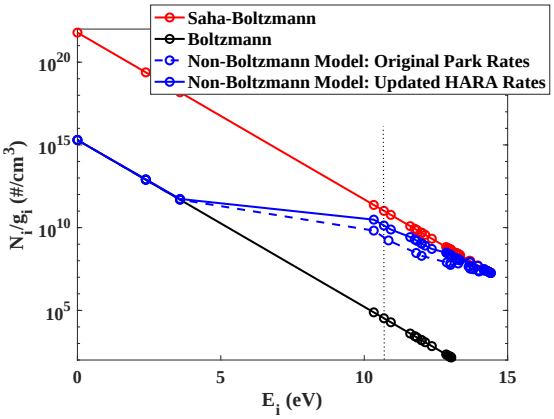

Fig. 6 Comparison of the electronic state populations for N at a condition representative of the backshell.

Note that characteristics of backshell radiation discussed in this section are unique to atomic line dominated conditions. For example, backshell radiation for Mars [31] and Titan [32] entry, which are typically at entry velocities below 8 km/s, are the result of molecular band emission from the near-shock flow within the field of view of the

backshell. The CO_2 and CH_4 present in the free-stream for Mars and Titan, respectively, result in strong post-shock nonequilibrium emission from CO_2 and CN at normal shock velocities below 3 km/s. These normal shock velocities are present for the oblique bow shock that is within the field of view of the backshell [33]. For CO_2, Sahai et al. [34] show that the recombination process of CO and O back to CO_2 does not provide an increase in the radiation analogous to the recombination of N^+ and e^- because of the close spacing of energy levels involved in each rovibrational transition. Therefore, only the near shock flow, which behaves identically to the post-shock nonequilibrium flow characteristic of the forebody radiation, provides noticeable radiation.

The discussion presented in this section is based on the Johnston and Brandis paper [1], which provides further details of backshell radiation for Earth entry. That paper also showed that the backshell calorimeter measurements of Fire II, which measured the convective plus radiative heating, supported the addition of a backshell radiation component. This experimental justification, along with the ability of the above discussion to explain the difference between the forebody and backshell radiation using fundamental relationships, provided a level of confidence in the backshell radiation component. This encouraged the radiative heating component to be included in the Osiris-Rex design analysis, which represented the first time backshell radiative heating was included for the design of an Earth entry vehicle.

IV. Development of the Radiative Heating Database for Artemis

Once the arguments for backshell radiation presented in the previous section were finalized, the possible importance of this heating component for the Artemis-1 Orion capsule was investigated. This was done based on the suggestion and assistance of Richard Thompson of NASA Langley Research Center, who was the Langley point-of-contact for Orion aerothermal. The three-dimensional angle of attack flowfields required for Orion are more computationally expensive than the axisymmetric Stardust or Osiris-Rex cases, so a single Artemis case was considered initially. The resulting convective and radiative heating are presented in Fig. 7. This result shows that radiative heating provides the dominant heating contribution to the separated lee-side backshell, where the convective heating is weak. The contribution of radiative heating to the wind-side is also shown to be of similar magnitude to the convective heating. This result strongly suggested that radiative heating should be included for the backshell of Orion, where it was currently being ignored based on the rationale presented in Section II. This conclusion was presented to the Orion Aerothermal Lead Adam Amar of the NASA Johnson Space Center. Recognizing the potential impact of this proposed radiative heating component, he requested that the evaluation of a new radiative heating database that included backshell radiation. Because the final backshell heating environments used for the Artemis-1 Orion backshell TPS was due in a few months, this new radiation database had to be developed quickly.

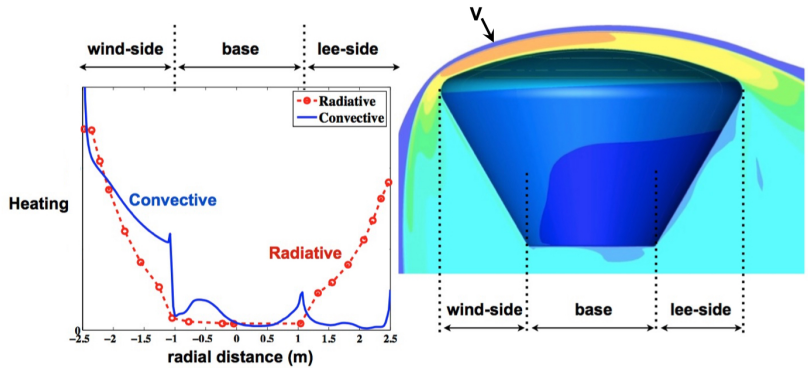

Fig. 7 Initial backshell radiative heating simulation for Orion at Artemis-1 conditions.

In addition to the challenge of developing the database quickly, accurate backshell radiative heating simulations at Artemis-1 conditions introduce further challenges relative to standard CFD simulations. The two primary challenges are the treatment of coupled radiation and the three-dimensional evaluation of the radiative transport equations [35]. The coupled radiation is required to account for radiative cooling [36], which had previously been treated using the approximate Tauber-Wakefield approach [37]. This Tauber-Wakefield approach is a post-processing step to an uncoupled radiation simulation. It is accurate only in the stagnation region, which makes it insufficient for backshell radiation predictions. The three-dimensional radiation transport approach was required to account for the non-tangent slab geometry of the backshell flowfield. The tangent slab approximation had been used for previous radiation databases

due to its computational efficiency and sufficient accuracy on the forebody [38]. The efficiency of the tangent slab approach is due to it requiring the evaluation of the radiative transport equations along a single line of sight for a given surface location. In contrast, a three-dimensional radiative transport approach, such as ray-tracing, requires hundreds of lines-of-sight for a single surface location. A database of ray-tracing radiative heating values that cover the forebody and backshell surface, computed for a coupled radiation flowfield, had never previously been evaluated both because of the computational expense and because the required codes had not yet been developed. However, recent developments to the LAURA flowfield and HARA radiation codes provided these capabilities and made these simulations feasible. The HARA code was developed to maintain computational efficiency and accuracy through the use of an adaptive spectral grid for atomic lines and the smeared band approach [39, 40] for optically-thin molecular band systems. This efficiency makes the coupling of HARA to the LAURA flowfield relatively trivial [41]. This efficiency also makes the numerous ray evaluations required by the ray-tracing approach over the entire surface of a vehicle computationally feasible, although the ray-tracing code for LAURA/HARA was not available until Alireza Mazaheri of NASA Langley Research Center had developed it in time for the Osiris-Rex analysis [42].

This new LAURA/HARA capability was used to compute the three-dimensional coupled radiation flowfields for Orion, followed by ray-tracing radiative heating computations at 279 surface points as a post-processing step to those flowfields. These simulations were performed for 129 cases, which covered a range of velocities, altitudes, and angles of attack. This database was completed in the two month timeframe required by the Orion/Artemis schedule. The margins applied to these forebody radiative heating values were developed by Brett Cruden and Aaron Brandis [43] of NASA Ames Research Center, which utilized recent EAST shock-tube measurements [44] and a novel approach for combining uncertainties from various sources.

While this radiation database was being computed, validation efforts reassessed the Fire II simulations initially considered by Johnston and Brandis [1]. The Johnston and Brandis analysis was intended to show that adding a radiative heating component to the convective component improved the comparison with the calorimeter measurement, which was achieved. The goal was not to claim that the radiative heating predictions were necessarily accurate. To inform the Orion database, a more detailed analysis was performed, where the magnitude of the radiative heating required to match the calorimeter database was considered. These simulations, performed by Victor Lessard of NASA Langley Research Center, used updated time-averaged flowfield simulations and a partially catalytic model tuned to match the convective heating late in trajectory when radiative heating was known to be negligible. A similar analysis was performed for the wind-side backshell of Apollo 4. Both the Fire II and Apollo 4 backshell calorimeter measurements [5, 45] showed improved comparisons with simulations if the predicted radiative heating values were reduced by roughly 50%. It was noted that this 50% reduction was within the parametric uncertainty bounds based on an analysis by Thomas West of NASA Langley Research Center, which represented an early version of the analysis presented in West et al. [46]. The large parametric uncertainty in the backshell radiative heating shown by West et al. was due mostly to non-Boltzmann rate uncertainties. As a result of these analyses, it was decided to reduce the nominal backshell radiative heating values in the database by 50%. This somewhat aggressive decision will be shown to be prescient.

V. Relevant Studies in Intermediate Years Between Design and Flight

Between the completion of the radiative heating database in 2015 and the flight of Artemis-1 in late 2022, there was significant work performed at NASA and universities to better understand the new Earth entry aerothermodynamic modeling challenge represented by backshell radiative heating. It remained conceivable that enough uncertainty existed in the HARA non-Boltzmann model that the actual backshell radiative heating was negligible, which would imply that the efforts described in the previous section were unnecessary. While the experimental and computational studies performed in these intermediate years would not be able to impact the Orion design, they could provide more evidence for the existence (or lack thereof) of this heating component or further support for the 50% reduction of the baseline LAURA/HARA backshell radiation values.

A computational study presented by Johnston and Panesi [47] treated the electronic levels of N as individual species in the LAURA flowfield simulations, which allowed the so-called quasi-steady-state approximation required [48] when computing the electronic populations as a flowfield post-processing step, to be avoided. This work leveraged Panesi's experience with this modeling approach developed in previous work [49]. Somewhat unexpectedly, the primary impact of this state-specific flowfield (SSF) model was on the two temperature modeling. The SSF model resulted in 20-40% lower backshell radiative heating than the conventional approach.

A study by Lopez et al. [50] reviewed the non-Boltzmann rates available up to that time in 2016 and compiled a revised rate model. The revised model resulted in even higher populations of strongly radiating levels relative to the HARA model used for the Artemis database.

An experimental study presented by Wei et al. [51] used the expansion tube at the University of Queensland to measure the air radiation to the backshell of a model. These measurements showed notable VUV emission to the backshell of the model, which was actually larger than predictions for some cases.

An experimental study by Tibere-Inglesse et al. [52–54] at the CentraleSupelec measured VUV emission from the expanding flow of a water-cooled test section placed on a plasma torch. These measurements allowed electronic state populations of N to be assessed at conditions representative of the backshell condition presented in Fig. 4. The resulting measurements confirmed the behavior shown in this figure, where the upper levels converge to the Saha-Boltzmann values, which are larger than the Boltzmann values. These measurements were used by Mariotto to develop an improved non-Boltzmann model [55, 56].

The studies reviewed in this section strengthened the argument for the existence of backshell radiation. However, considering all of the studies together, their conclusion regarding the magnitude of the radiation was inconclusive. This means they did not provide definitive additional support for the 50% reduction to the nominal LAURA/HARA values. As a result, the return of the Orion capsule from the Artemis-1 mission and the assessment of the backshell heating implied by its thermocouples was highly anticipated.

VI. Comparison with Artemis-1 Measurements

Artemis-1 successfully reentered Earth's atmosphere on December 11, 2022. Thermocouples on the backshell TPS allowed the total heating (convective plus radiative) to be reconstructed from the measured temperature time histories. The Orion Aerothermal Team performed this reconstruction. They also obtained the reconstructed trajectory and applied it to the aeroheating database [57], which included the radiative heating component discussed in this paper. The database values for the convective heating were computed by the Orion Aerothermal Team, which represented separate flowfield simulations than those used for the radiative heating database.

The resulting database heating values are compared in Fig. 8 with the heating inferred from the thermocouple measurements (the present discussion is limited to the lee-side of the backshell since it is expected to have seen the largest impact from radiative heating). The spikes in the distribution are from the reaction control system, and are not relevant to this discussion. Also, the axes are removed from the figure to meet export control requirements. This figure shows that the radiative heating component is required for the total simulated heating to match the measurements. If radiation was not included, the heating to the lee-side surface region near the top of this figure would have been under-predicted by over a factor of two in the peak heating region of the trajectory. It is beyond the scope of this work to speculate about the potential consequences of the TPS design using convective heating only. At the very least, significant analysis would have been required prior to the crewed Artemis-2 mission to demonstrate that the as-built backshell, which is the same as Artemis-1, was sufficient due to other (non-aeroheating) design margins. Fortunately, the inclusion of backshell radiation for the Artemis-1 design allows this situation to be avoided.

The radiative heating values presented in Fig. 8 include the 50% reduction to the baseline LAURA/HARA (backshell only) radiation values previously discussed. The slight over-prediction of the total heating for most cases indicate that this was an excellent assumption. A future paper will re-compute the backshell radiative heating using model updates made since 2015, although it is noted that these updated models are able to capture most of this 50% reduction.

VII. Summary

The backshell radiative heating for Earth entry was ignored primarily because of the negligible Fire and Apollo 4 backshell radiometer measurements and negligible radiative heating resulting from the assumed upper-limit Boltzmann assumption of atomic electronic levels. These assumptions are shown to be erroneous in the recombining expanding flow characteristic of the wake, where the slow finite-rate recombination of electrons and ions leads to the Saha-Boltzmann distribution being larger than the Boltzmann distribution. Because the non-Boltzmann model leads to upper levels of VUV lines near the Saha-Boltzmann limit while the lower levels are near the Boltzmann limit, the resulting VUV radiation is larger than if the upper levels were in a Boltzmann distribution. This observation confirms that the backshell radiation is dominated by VUV atomic lines and assuming a Boltzmann distribution results in the lower limit for the backshell radiation instead of the upper limit. Since the VUV region of the spectrum was not included in the Fire and Apollo 4 backshell radiometer measurements because the VUV was absorbed by the quartz window, this explains

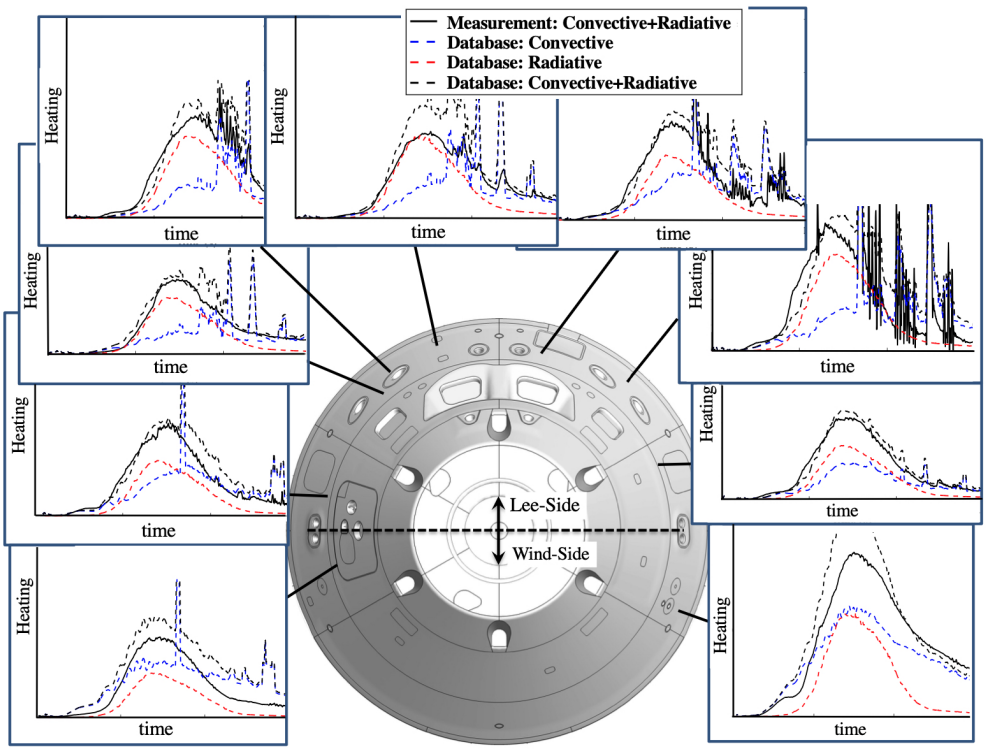

Fig. 8 Comparison between measurement reconstructed heating and un-margined database values for Artemis-1.

their negligible measured values. Once the erroneous nature of the negligible backshell radiation assumption was recognized during the analysis of Osiris-Rex, a backshell radiative heating database was swiftly implemented in the aeroheating database for Artemis-1, just prior to the final backshell TPS sizing. The return of the Orion capsule for Artemis-1 in December 2022 provided backshell thermocouple measurements, which allowed the total backshell heating to be inferred. These measurements confirmed that including the radiative heating component of the backshell lee-side avoided a significant under-prediction in the heating used for design.

References

[1] Johnston, C. O., and Brandis, A. M., "Features of Afterbody Radiative Heating for Earth Entry," *Journal of Spacecraft & Rockets*, Vol. 52, No. 1, 2015, pp. 105–119.

[2] Meyerott, R. E., "Radiation Heat Transfer to Hypersonic Vehicles," Third AGARD Combustion and Propulsion Panel Colloquium, 1958.

[3] Reid, R. C., Rochelle, W. C., and Milhoan, J. D., "Radiative Heating to the Command Module: Engineering Prediction and Flight Measurement," NASA TM-X 58091, 1972.

[4] Cauchon, D. L., "Radiative Heating Results from the Fire II Flight Experiment at a Reentry Velocity of 11.4 Kilometers Per Second," NASA TM X 1402, Jul. 1967.

[5] Lee, D. B., and Goodrich, W. D., "The Aerothermodynamic Environment of the Apollo Command Module During Superorbital Entry," NASA TN 6792, 1972.

[6] Park, C., "Radiation Enhancement by Nonequilibrium in Earth's Atmosphere," *Journal of Spacecraft & Rockets*, Vol. 22, No. 1, 1985, pp. 27–36.

[7] Gnoffo, P. A., "An Upwind-Biased, Point-Implicit Relaxation Algorithm for Viscous, Compressible Perfect-Gas Flows," NASA TP 2953, Feb. 1990.

[8] Gnoffo, P. A., Gupta, R. N., and Shinn, J. L., "Conservation Equations and Physical Models for Hypersonic Air Flows in Thermal and Chemical Nonequilibrium," NASA TP 2867, Feb. 1989.

[9] Wright, M. J., Candler, G. V., and Bose, D., "A Data-Parallel Line Relaxation Method of the Navier-Stokes Equations," AIAA Paper 1997-2046, 1997.

[10] Gnoffo, P. A., Weilmuenster, K. J., Hamilton, H. H., Olynick, D. A., and Venkatapathy, E., "Computational Aerothermodynamic Design Issues for Hypersonic Vehicles," *Journal of Spacecraft & Rockets*, Vol. 36, No. 1, 1999, pp. 21–43.

[11] Park, C., "Nonequilibrium Air Radiation (NEQAIR) Program: User's Manual," NASA TM 86707, 1985.

[12] Park, C., *Nonequilibrium Hypersonic Aerothermodynamics*, 1st ed., Wiley, New York, 1990.

[13] Park, C., "Comparison of Electron and Electronic Temperatures in a Recombining Nozzle Flow of Ionized Nitrogen Hydrogen Mixture. Part 1. Theory," *Journal of Plasma Physics*, Vol. 9, 1973, pp. 187–215.

[14] Park, C., "Comparison of Electron and Electronic Temperatures in a Recombining Nozzle Flow of Ionized Nitrogen Hydrogen Mixture. Part 2. Experiment," *Journal of Plasma Physics*, Vol. 9, 1973, pp. 217–234.

[15] Sohn, I., Li, Z., and Levin, D. A., "Effect of Escape Factor to a Hypersonic Nonequilibrium Flow Implemented in DSMC Photon Monte Carlo Radiation," *Journal of Thermophysics and Heat Transfer*, Vol. 26, No. 3, 2012, pp. 393–406.

[16] Olynick, D., Chen, Y.-K., and Tauber, M. E., "Aerothermodynamics of the Stardust Sample Return Capsule," *Journal of Spacecraft & Rockets*, Vol. 36, No. 3, 1999, pp. 442–462.

[17] Fujita, K., Abe, T., and Suzuki, K., "Air Radiation Analysis of a Superorbital Reentry Vehicle," AIAA Paper 1997–2561, 1997.

[18] Otsu, H., Suzuki, K., Fujita, K., and Abe, T., "Assessment of Forebody and Backbody Radiative Heating Rate of Hypervelocity Reentry Capsule," ISAS Report SP 17, 2003.

[19] Liu, Y., Prabhu, D., Saunders, D., Vinokur, M., and Dateo, C., "Comparison of Tangent Slab Approximation and Full Angular Integration in Computing Radiative Heating for the CEV Heatshield," NASA TN/EG CAP-06-124, 2006.

[20] Erb, R. B., Greenshields, D. H., Chauvin, L. T., Pavlosky, J. E., and Statham, C. L., "Apollo Thermal Protection System Development," *Journal of Spacecraft & Rockets*, Vol. 7, No. 6, 1970, pp. 727–734.

[21] Pavlosky, J. E., and Leger, L. G. S., "Apollo Experience Report - Thermal Protection Subsystem," NASA TN-D 7564, 1974.

[22] Erb, R. B., Lee, D. B., Weston, K. C., and Greenshields, D. H., "Aerothermodynamics–The Apollo Experience," *Proceedings of the 1967 Heat Transfer and Fluid Mechanics Institute*, Stanford University Press, 1967.

[23] Wright, M., Milos, F., and Tran, P., "Afterbody Aeroheating Flight Data for Planetary Probe Thermal Protection System Design," *Journal of Spacecraft & Rockets*, Vol. 43, No. 5, 2006, pp. 929–943.

[24] Schneider, S. P., "Laminar-Turbulent Transition on Reentry Capsules and Planetary Probes," *Journal of Spacecraft & Rockets*, Vol. 43, No. 6, 2006, pp. 1153–1173.

[25] Space-Division-North-American-Rockwell, "Certification Analysis, CAR 02001B, Apollo Block II Heat Shield, Volume II, Entry Environments," SD 68-1004-2, 1969.

[26] Harris, R., Stewart, M., and Koenig, W., "Thermal Protection System Technology Transfer from Apollo and Space Shuttle to the Orion Program," AIAA Paper 2018–5134, 2018.

[27] Johnston, C. O., Hollis, B., and Sutton, K., "Non-Boltzmann Modeling for Air Shock Layers at Lunar Return Conditions," *Journal of Spacecraft & Rockets*, Vol. 45, 2008, pp. 879–890.

[28] Frost, R. M., "Calculated Cross Sections and Measured Rate Coefficients for Electron-Impact Excitation of Neutral and Singly Ionized Nitrogen," *Journal of Applied Physics*, Vol. 84, 1998, pp. 2989–3003.

[29] Tayal, S. S., "Effective Collision Strengths for Electron Impat Excitation of N I," *Atomic Data and Nuclear Data Tables*, Vol. 76, No. 2, 2000, pp. 191–212.

[30] Lauretta, D. S., Balram-Knutson, S. S., and Beshore, E., "OSIRIS-REx: Sample Return from Asteroid (101955) Bennu," *Space Sci Rev*, Vol. 212, 2017, p. 925–984. doi:https://doi.org/10.1007/s11214-017-0405-1.

[31] Brandis, A. M., Saunders, D. A., Johnston, C. O., Cruden, B. A., and White, T. R., "Radiative Heating on the After-Body of Martian Entry Vehicles," *Journal of Thermophysics and Heat Transfer*, Vol. 34, No. 1, 2020, pp. 66–77.

[32] Johnston, C. O., West, T. K., and Brandis, A. M., "Features of Afterbody Radiative Heating for Titan Entry," AIAA paper 2019-3010, 2019. doi:10.2514/6.2019-3010.

[33] Johnston, C. O., "Evaluating Shock-Tube Informed Biases for Shock-Layer Radiative Heating Simulations," *Journal of Thermophysics and Heat Transfer*, Vol. 35, No. 2, 2021, pp. 349–361.

[34] Sahai, A., Johnston, C. O., Lopez, B., and Panesi, M., "Flow-Radiation Coupling in CO_2 Hypersonic Wakes using Reduced-Order Non-Boltzmann Models," *Physical Review Fluids*, Vol. 4, 2019, p. 093401.

[35] Hartung, L. C., and Hassan, H. A., "Radiation Transport Around Axisymmetric Blunt Body Vehicles Using a Modified Differential Approximation," *Journal of Thermophysics and Heat Transfer*, Vol. 7, No. 2, 1993, pp. 220–227.

[36] Goulard, R., "The Coupling of Radiation and Convection in Detached Shock Layers," *Journal of Quantitative Spectroscopy and Radiative Transfer*, Vol. 1, 1961, pp. 249–257.

[37] Tauber, M. E., and Wakefield, R. M., "Heating Environment and Protection During Jupiter Entry," *Journal of Spacecraft & Rockets*, Vol. 8, No. 6, 1971, pp. 630–636.

[38] Johnston, C. O., "Improved Exponential Integral Approximation for Tangent-Slab Radiation Transport," *Journal of Thermophysics and Heat Transfer*, Vol. 24, No. 3, 2010, pp. 659–661.

[39] Chambers, L. H., "Predicting Radiative Heat Transfer in Thermochemical Nonequilibrium Flow Fields," NASA TM 4564, 1994.

[40] Johnston, C. O., Hollis, B. R., and Sutton, K., "Spectrum Modeling for Air Shock-Layer Radiation at Lunar-Return Conditions," *Journal of Spacecraft & Rockets*, Vol. 45, 2008, pp. 865–878.

[41] Johnston, C. O., Gnoffo, P. A., and Sutton, K., "Influence of Ablation on Radiative Heating for Earth Entry," *Journal of Spacecraft & Rockets*, Vol. 46, No. 3, 2009, pp. 481–491.

[42] Mazaheri, A., Johnston, C., and Sefidbakht, S., "Three-Dimensional Radiation Ray-Tracing for Shock Layer Radiative Heating Simulations," *Journal of Spacecraft & Rockets*, Vol. 50, No. 3, 2013.

[43] Cruden, B. A., Brandis, A. M., and Johnston, C. O., "Development of a Radiative Heating Margin Policy for Lunar Return Missions," *Journal of Thermophysics and Heat Transfer*, Vol. 32, No. 1, 2018, pp. 303–315.

[44] Brandis, A. M., and Cruden, B. A., "Benchmark Shock Tube Experiments of Radiative Heating Relevant to Earth Re-entry," AIAA Paper 2017–1145, 2017.

[45] Slocumb, T. H., "Project Fire II Afterbody Temperature and Pressures at 11.35 Kilometers Per Second," NASA TM X 1319, Dec. 1966.

[46] West, T. K., Johnston, C. O., and Hosder, S., "Uncertainty and Sensitivity Analysis of Afterbody Radiative Heating Predictions for Earth Entry," *Journal of Thermophysics and Heat Transfer*, Vol. 31, No. 2, 2017, pp. 294–306.

[47] Johnston, C. O., and Panesi, M., "Impact of state-specific flowfield modeling on atomic nitrogen radiation," *Physical Review Fluids*, Vol. 1, 2018, p. 013402.

[48] Park, C., *Nonequilibrium Hypersonic Aerothermodynamics*, 1st ed., Wiley, 1990.

[49] Panesi, M., and Lani, A., "Collisional Radiative Coarse-Grain Model for Ionization in Air," *The Physics of Fluids*, Vol. 25, 2013, p. 057101.

[50] Lopez, B., Johnston, C. O., and Panesi, M., "Improved Non-Boltzmann Modeling for Nitrogen Atoms," AIAA Paper 2016–4431, 2016.

[51] Wei, H., Morgan, R. G., McIntyre, T. J., Brandis, A. M., and Johnston, C. O., "Experimental and Numerical Investigation of Air Radiation in Superorbital Expanding Flow," AIAA Paper 2018–4531, 2018.

[52] Tibère-Inglesse, A. C., McGuire, S. D., Mariotto, P., and Laux, C. O., "Validation Cases for Recombining Nitrogen and Air Plasmas," *Plasma Sources Science and Technology*, Vol. 27, No. 11, 2018, p. 115010.

[53] Tibère-Inglesse, A. C., McGuire, S. D., and Laux, C. O., "Nonequilibrium Radiation from a Recombining Nitrogen Plasma," AIAA Paper 2018–0241, 2018.

[54] Tibère-Inglesse, A. C., McGuire, S. D., and Laux, C. O., "Atomic Radiation from a Recombining Nitrogen Plasma," AIAA Paper 2019–2068, 2019.

[55] Mariotto, P., Tibère-Inglesse, A. C., Gollan, R., Jacobs, P., Perrin, M.-Y., and Laux, C. O., "Atomic State-to-State Modeling of Ionization Nonequilibrium in a Recombining Plasma," AIAA Paper 2020–1713, 2020.

[56] Marriotto, P., "Kinetics of Nonequilibrium Recombining Nitrogen-Argon Plasmas," *Ph.D. Disseration*, Paris-Saclay University, 2023.

[57] Orion Aerothermal Team, "Orion Aerothermal Substantiation Report," NASA Internal Report, 2019.